

Ethane and methane at high pressures: Structure and stability

Cite as: J. Chem. Phys. **155**, 184503 (2021); <https://doi.org/10.1063/5.0067828>

Submitted: 20 August 2021 • Accepted: 19 October 2021 • Accepted Manuscript Online: 20 October 2021 • Published Online: 11 November 2021

 Elissaios Stavrou,  Alexander A. Maryewski,  Sergey S. Lobanov, et al.



View Online



Export Citation



CrossMark

ARTICLES YOU MAY BE INTERESTED IN

[Carbon-carbon supercapacitors: Beyond the average pore size or how electrolyte confinement and inaccessible pores affect the capacitance](#)

The Journal of Chemical Physics **155**, 184703 (2021); <https://doi.org/10.1063/5.0065150>

[The microscopic origin of the anomalous isotopic properties of ice relies on the strong quantum anharmonic regime of atomic vibration](#)

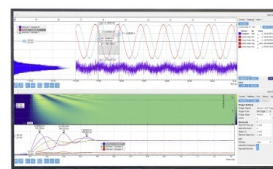
The Journal of Chemical Physics **155**, 184502 (2021); <https://doi.org/10.1063/5.0062689>

[Conditions for electroneutrality breakdown in nanopores](#)

The Journal of Chemical Physics **155**, 184701 (2021); <https://doi.org/10.1063/5.0070178>

Challenge us.

What are your needs for
periodic signal detection?



Zurich
Instruments

Ethane and methane at high pressures: Structure and stability

Cite as: *J. Chem. Phys.* **155**, 184503 (2021); doi: [10.1063/5.0067828](https://doi.org/10.1063/5.0067828)

Submitted: 20 August 2021 • Accepted: 19 October 2021 •

Published Online: 11 November 2021



View Online



Export Citation



CrossMark

Elissaios Stavrou,^{1,2,3,a)} Alexander A. Maryewski,⁴ Sergey S. Lobanov,^{1,5} Artem R. Oganov,⁴ Zuzana Konôpková,^{6,7} Vitali B. Prakapenka,⁸ and Alexander F. Goncharov^{1,b)}

AFFILIATIONS

¹ Earth and Planets Laboratory, Carnegie Institution of Washington, Washington, DC 20015, USA

² Materials and Engineering Science Program, Guangdong Technion-Israel Institute of Technology, Shantou, Guangdong 515063, China

³ Technion-Israel Institute of Technology, Haifa 32000, Israel

⁴ Skolkovo Institute of Science and Technology, 3 Nobel St., Moscow 143026, Russian Federation

⁵ GFZ German Research Center for Geosciences, Section 3.6, Telegrafenberg, 14473 Potsdam, Germany

⁶ DESY Photon Science, D-22607 Hamburg, Germany

⁷ European XFEL GmbH, Holzkoppel 4, D-22869 Schenefeld, Germany

⁸ Center for Advanced Radiation Sources, University of Chicago, Chicago, Illinois 60637, USA

^{a)} Author to whom correspondence should be addressed: elissaios.stavrou@gtit.edu.cn

^{b)} Electronic mail: agoncharov@carnegiescience.edu

ABSTRACT

We have performed a combined experimental and theoretical study of ethane and methane at high pressures of up to 120 GPa at 300 K using x-ray diffraction and Raman spectroscopies and the USPEX *ab initio* evolutionary structural search algorithm, respectively. For ethane, we have determined the crystallization point, for room temperature, at 2.7 GPa and also the low pressure crystal structure (phase A). This crystal structure is orientationally disordered (plastic phase) and deviates from the known crystal structures for ethane at low temperatures. Moreover, a pressure induced phase transition has been identified, for the first time, at 13.6 GPa to a monoclinic phase B, the structure of which is solved based on good agreement with the experimental results and theoretical predictions. For methane, our x-ray diffraction measurements are in agreement with the previously reported high-pressure structures and equation of state (EOS). We have determined the EOSs of ethane and methane, which provides a solid basis for the discussion of their relative stability at high pressures.

Published under an exclusive license by AIP Publishing. <https://doi.org/10.1063/5.0067828>

I. INTRODUCTION

Methane is one of the most abundant hydrocarbon molecules in the universe and is expected to be a significant part of the icy giant planets (Uranus and Neptune) and their satellites.^{1,2} Ethane is one of the most predictable products of chemical reactivity of methane at extreme pressures and temperatures.^{3–6} Moreover, the broad range of thermodynamic conditions at which hydrocarbons are present in the universe (from below 100 to 10 000 K and pressures of up to 1 TPa) determines the importance of understanding the physics and chemistry of hydrocarbons at extreme pressure and temperature. Both methane and ethane have been found in the planetary atmospheres.⁷

Despite numerous experimental and theoretical studies,^{8–16} the structure and relative stability of methane and other hydrocarbons¹⁷ at high pressures, even at room temperature, remain controversial even at moderate pressures. At room temperature (RT), methane solidifies in a plastic fcc phase (orientationally disordered) that is stable up to 5.4 GPa.¹⁸ At higher pressures, methane adopts orientationally disordered (based on the Raman spectroscopy data that show splitting of the C–H stretch modes^{8,13}) phases: (a) a rhombohedral structure (phase A) up to 9 GPa and (b) a cubic structure (phase B) up to 25 GPa.^{9,10} The hydrogen positions could have been determined only for phase A (below 9 GPa). A phase must be disordered based on the account of splitting of the ν_1 and ν_3 modes. The authors of Ref. 9 (neutron and x-ray diffraction measurements) suggested

that it may be partially ordered. The transition between phase A and phase B is very sluggish; if pressure is increased quickly, yet another phase named pre-B is formed, which shows Raman spectra similar to phase A and x-ray diffraction (XRD) patterns similar to phase B.⁸ The exact structure of the high-pressure (HP) phase above 25 GPa is unknown. It was proposed that methane would behave as a “bad” noble gas and assume an hcp structure at high pressure.¹⁹ However, the structure of methane can be well indexed by a cubic phase of up to 202 GPa.¹² In the later study, two distinct cubic phases, namely, a simple cubic (SC) stable up to 94 GPa and high-pressure cubic (HP-C), were reported.

In contrast to rather rich data on methane, very little is known about the crystal structure of ethane at high pressure.^{4,6,20–22} A very recent experimental study using Raman spectroscopy²² reported a series of phase transitions of ethane of up to 120 GPa at RT; however, no structural characterization was provided. Theoretical structure search, which includes a possible composition change between various hydrocarbons, suggests that methane is stable to almost 100 GPa,⁵ while at higher pressures other substances become stable—such as ethane, butane, methane–hydrogen compounds (CH₄)₄(H₂)₂ and (CH₄)₂(H₂)₃ (similar to those reported at lower pressures²³), and molecular H₂.²⁴ Above 300 GPa, the only stable phases are H₂ and diamond in qualitative agreement with the earlier work.³ All these phases can be metastable in a wide pressure range, and the kinetic hindrance can be overcome via a high-temperature treatment. However, nominally metastable at low temperatures, hydrocarbon phases (e.g., ethane) can be synthesized at high P–T conditions,^{4,6} which have been argued to stabilize at pressure and/or temperature, additionally helped by a catalytic reaction.²⁵

To address the structure and the composition of hydrocarbons at high pressures, we have performed a combined experimental, using x-ray diffraction (XRD) and Raman spectroscopies, and theoretical, using the USPEX *ab initio* evolutionary structural search algorithm,^{14,24} study of both methane and ethane up to megabar pressures at room temperature (RT). For ethane, we have determined the crystallization point, for room temperature, at 2.7 GPa and also the low pressure crystal structure (phase A), in agreement with Ref. 21. This crystal structure is orientationally disordered (plastic phase) and deviates from the known crystal structures for ethane at low temperatures.^{26,27} In addition, a pressure induced phase transition has been identified, for the first time, at 13.6 GPa to a monoclinic phase B, the structure of which is solved based on good agreement with the experimental results and theoretical predictions. This phase is isostructural with phase III, previously reported at low temperatures.²⁶ We have determined the equations of state (EOSs) of ethane and methane up to Mbar pressures, which provides a solid basis for the discussion of their relative stability at high pressures.

II. METHODS

A. Experimental methods

Methane and ethane (both with nominal purity better than 99.9995%) were loaded into a diamond anvil cell (DAC) with the use of a gas loading apparatus, where a gas pressure of about 0.2 GPa was created. Small quantities of ruby and gold powder were also loaded for the determination of pressure through ruby luminescence and gold EOS, respectively.^{28,29} XRD data were collected at the

GeoSoilEnviroCARS (sector 13), Advanced Photon Source (APS), Chicago, and Extreme Conditions Beamline P02.2 at DESY (Germany). Cubic boron nitride (c-BN) gaskets were used for the Mbar XRD measurements. This allows for larger sample volumes, given that both methane and ethane are weak scatterers. Moreover, the use of c-BN gasket prevents “contamination” of XRD patterns from rhenium peaks, which are usually present at high pressures.^{8,12} Raman studies were performed using 488 and 532 nm lines of a solid-state laser. Raman spectra were analyzed with a spectral resolution of 4 cm⁻¹ using a single-stage grating spectrograph equipped with a CCD array detector.

Integration of powder diffraction patterns to yield scattering intensity vs 2θ diagrams and initial analysis were performed using the DIOPTAS program.³⁰ The calculated XRD patterns were produced using the POWDER CELL program³¹ for the corresponding crystal structures according to the EOSs determined experimentally and theoretically in this study and assuming continuous Debye rings of uniform intensity. Rietveld refinements were performed using the GSAS software.³² Indexing of XRD patterns has been performed using the DICVOL program³³ as implemented in the FullProf Suite.

B. Computational methods

The computational search for stable phases of ethane under pressure was performed using the USPEX evolutionary algorithm³⁴ in its version¹⁴ for molecular crystals. Force-field (UFF³⁵) optimized geometry of the ethane molecule was used as input for structure search. We explicitly considered structures with $Z = 2, 4, 8, 10, 12, 14,$ and 16 molecules per unit cell in all possible space groups. Generation size was set to 80 structures. External pressure was set to 30 GPa during the search. Each structure in USPEX search was relaxed using the Vienna *Ab initio* Simulation Package (VASP)^{36–38} with the Perdew–Burke–Ernzerhof (PBE)³⁹ functional (with D3 dispersion correction⁴⁰) and projector augmented wave (PAW) pseudopotentials⁴¹ in several consecutive steps with increasing precision, plane wave basis set cutoff, and number of points on the k-grid: finally, the most precise step was performed with a cutoff of 600 eV and $2\pi \times 0.09 \text{ \AA}^{-1}$ reciprocal space resolution (as defined in the original USPEX paper³⁴). Fitting of the Birch–Murnaghan EOS was done by relaxing the predicted ethane structure at ten equidistant pressure values in the 10–100 GPa range with 600 eV cutoff and 0.5 \AA^{-1} k-point spacing; the obtained equilibrium cell volumes and energies were used for a three-parameter fit.

III. RESULTS

A. High-pressure study of ethane

1. Raman spectroscopy

Figure 1 shows nonpolarized Raman spectra of ethane at the selected pressures of up to 40 GPa. Frequency pressure plots are shown in Fig. 2. Ethane crystallizes at about 2 GPa, determined by the appearance of lattice modes above solidification pressure. The Raman spectrum can be divided into three main spectral ranges: (i) from 2850 to 3100 cm⁻¹ attributed to C–H stretching vibrations,⁴² (ii) from 1000 to 1500 cm⁻¹ attributed to C–C stretching and C–H bending, and (iii) below 600 cm⁻¹ arising from lattice modes.

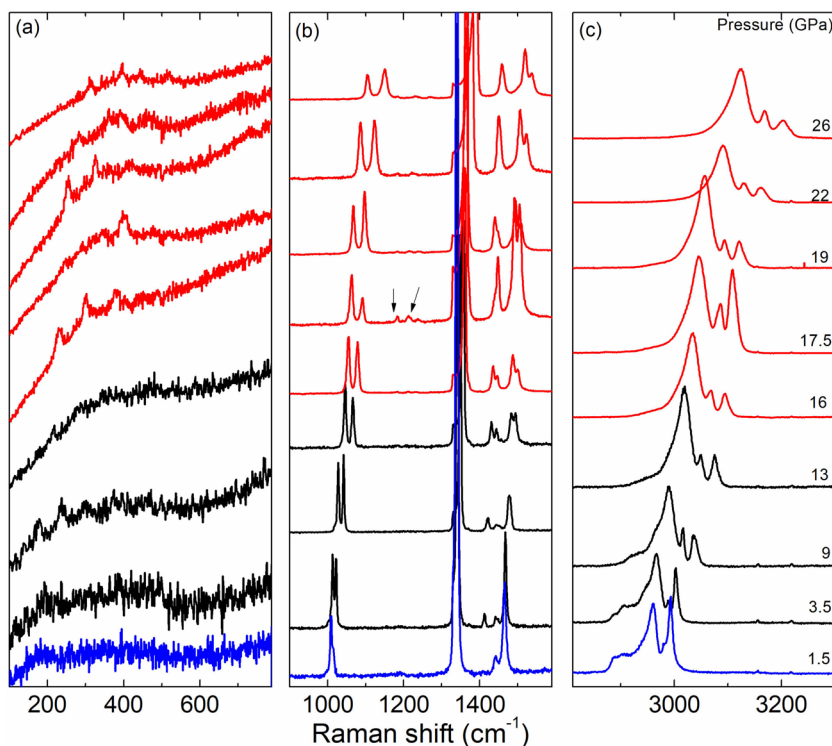


FIG. 1. Raman spectra of ethane at the selected pressures: (a) lattice modes, (b) C–C stretching and C–H bending modes, and (c) C–H stretching modes. The Raman spectra of the A and B phases are shown in black and red, respectively. The Raman spectrum of liquid ethane just below crystallization pressure is also shown in blue.

At above 13 GPa, a phase transition has been observed manifested by the decrease in the number of high-frequency C–H stretching modes with the parallel appearance of C–H bending modes at 1200 cm^{-1} (indicated by the arrows in Fig. 1). Moreover, an

increase in the number of the lattice modes (see Fig. 2) indicates a lower symmetry unit cell. No indication of additional phase transitions was observed up to the highest pressure of this study (40 GPa).

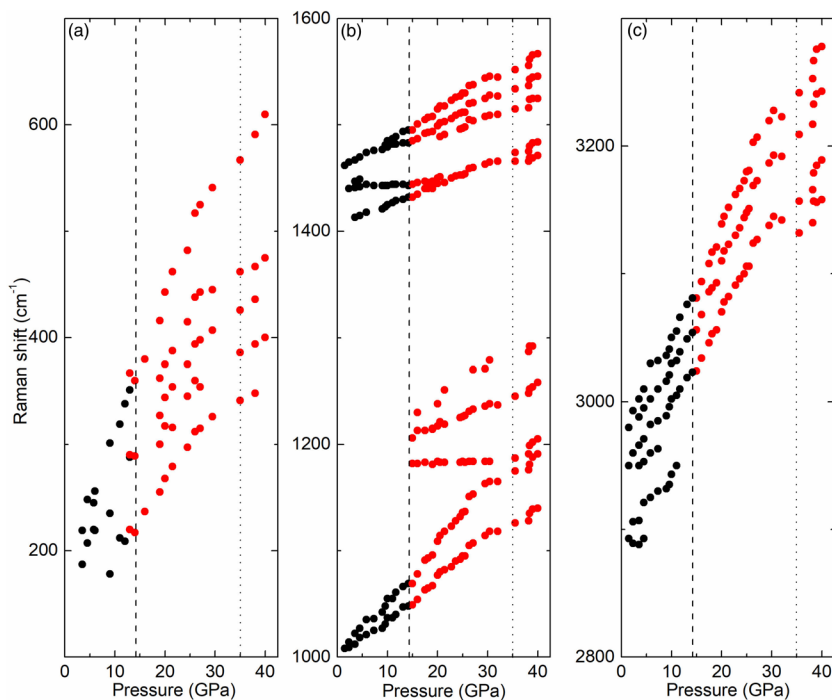


FIG. 2. Frequency vs pressure plots of the ethane Raman modes: (a) lattice modes, (b) C–C stretching and C–H bending modes, and (c) C–H stretching modes. The Raman mode frequencies of the A and B phases are shown in black and red, respectively. The vertical dashed and dotted lines indicate the critical pressures of the phase transitions (see the text for details) at 13 and 35 GPa, respectively.

With a further pressure increase, few spectral discontinuities in Raman mode frequencies and slopes, see Fig. 2, at 35 GPa indicate the presence of an additional transition, in agreement with the results of Ref. 22. Given that no new modes appear above this pressure, we tentatively attribute this transition as to be mainly associated with a possible isostructural transition. This is further justified by the absence of any indication of a phase transition in XRD measurements; see Sec. III A 2.

2. X-ray diffraction

Representative XRD patterns of ethane at various pressures are shown in Fig. 3. The crystalline phase (indicated as phase A in our study and phase IV in Ref. 21) of ethane at the lower pressure range (from crystallization of up to 13 GPa) cannot be indexed with the known crystalline phases at low temperatures. Indeed, both the plastic BCC (phase I) and the monoclinic ordered (phase III) phases reported previously^{26,27} have XRD patterns distinct from those observed in our study. With a pressure increase, a clear indication of a phase transition to a high pressure phase (indicated as phase B) has been observed at 13.4 GPa, in perfect agreement with Raman spectroscopy. No other phase transition has been observed up to 110 GPa.

In order to solve the crystal structures of both phases of ethane, we have performed a combined *ab initio* and experimental (indexing) procedure. We would like to point out that from experimental data, only carbon positions can be extracted from

experimental data due to the low scattering cross section of hydrogen atoms. The results of the analysis of the experimental results are as follows: (a) Phase A can be indexed with a tetragonal cell ($a = b = 5.11$ c = 3.74 Å at 5 GPa) in agreement with Ref. 21; (b) phase B is determined as a monoclinic structure [space group (S.G.) $P2_1/n$ ($Z = 2$)] with $a = 3.40$, $b = 4.66$, and $c = 4.76$ Å and $\beta = 90.45^\circ$ at 20 GPa; and (c) A and B phases should be closely related, most probably holding an orientation order–disorder relation with higher symmetry carbon positions in phase A. This is further justified by Raman spectroscopy, where an increased number of the low frequency lattice modes have been observed after the phase transition. The lattice mode frequencies of phase B seem to be on the extension of phase A dependencies; see Fig. 2(a). The increased number of the lattice modes and the appearance of the C–H bending modes suggest the symmetry lowering.

Computational search for ethane above 14 GPa produced 486 enthalpy-ranked structures, which were analyzed for matching the experimental XRD and cell parameters in the order of the enthalpy increase increasing enthalpy. The most stable (lowest enthalpy) structure found during the computational search immediately returned lattice parameters and XRD peak positions closely matching those of the experimentally found phase B; see Fig. 3. Slight discrepancies in Bragg peaks intensities are attributed to preferred orientation effects due to ethane solidification under pressure, resulting in an agglomeration of microdimensional single crystals. The next, theoretically predicted, low energy structure has an energy of 1.245 kcal/mol above this structure. The calculated lattice parameters of the lowest energy structure are $a = 3.22$, $b = 4.49$, $c = 4.52$, and $\beta = 90.47^\circ$ with $P2_1/n$ S.G. and $Z = 2$ at 30 GPa. We consider the similarity with the experimentally determined lattice parameters and S.G. sufficient to uniquely identify this structure as phase B. Interestingly, this structure was found to be the stable one in several independent searches. Close agreement between the experimentally and computationally determined structures of phase B of ethane gives us confidence that this should be the correct structure of ethane above 13 GPa. This is further justified by good agreement between the experimentally and computationally determined pressure dependence of the lattice parameters and the EOSs for phase B; see Figs. 4(a) and 4(b).

Our XRD experiments and theoretical calculations suggest that phase B is an orientationally ordered body centered tetragonal (BCT)-like structure (see the insets of Fig. 4), in which the ethane molecule at the center of the unit cell has an orientation (the direction of the C–C bond) perpendicular to the orientation of the molecules at the corners. This crystal structure resembles very much monoclinic phase III known from low temperature (LT) studies.²⁶ At 70 K and ambient pressure, phase III has lattice constants of $a = 4.226$, $b = 5.623$, and $c = 5.845$ Å and $\beta = 90.41^\circ$ with the same SG ($P2_1/n$) of phase B. Moreover, arrangement of ethane molecules is the same in both structures. Thus, it is plausible to assume, although no experimental data are available in the intermediate temperature and pressure region, that phase B is identical to LT phase III based on good agreement between lattice parameters and SG.

Using the above-mentioned structures, we have obtained the lattice parameters and the EOS of ethane of up to 110 GPa. The results are shown in Fig. 4. The pressure induced A \rightarrow B phase transition is accompanied by a slight ($\approx -2\%$) volume drop. The continuity

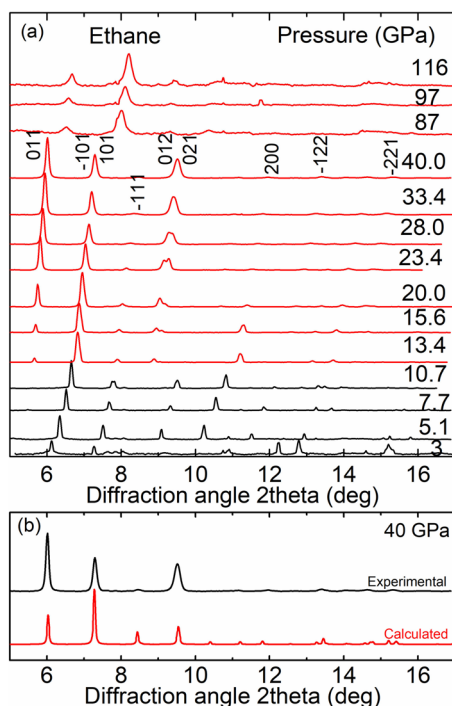


FIG. 3. (a) Selected XRD patterns of ethane on the pressure increase. The XRD patterns of A and B phases are shown in black and red, respectively. The Miller indices for phase B are noted. The x-ray wavelength is $\lambda = 0.3344$ Å. (b) Comparison between the experimental and calculated (theoretically predicted phase B) patterns of ethane.

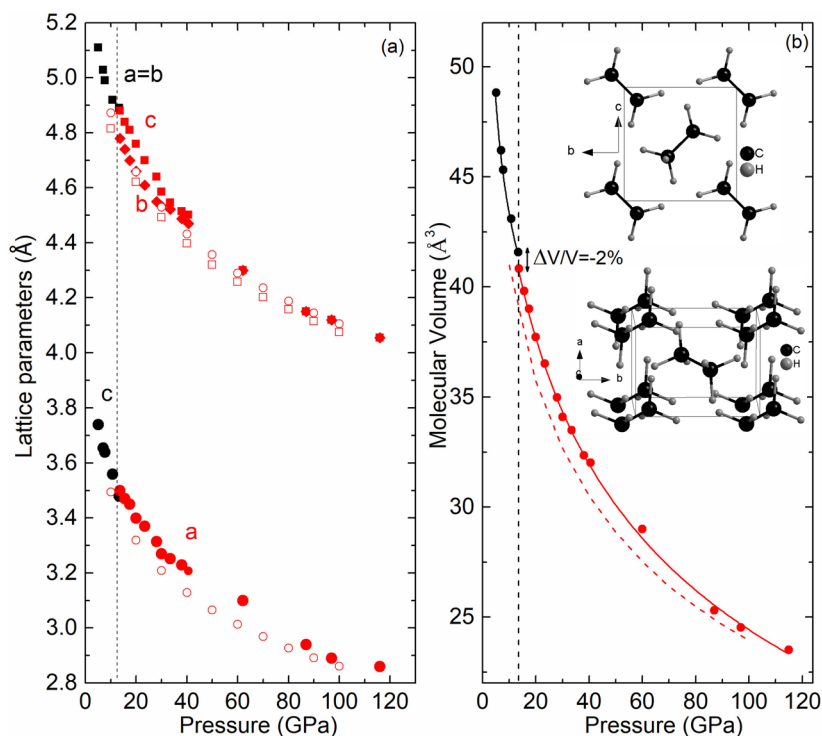


FIG. 4. Pressure dependence of (a) lattice parameters and (b) molecular volume of ethane. The dashed vertical lines denote the critical pressure for the phase transition. In (a), experimental and calculated results are plotted with the solid and open symbols, respectively. The solid lines in (b) are the unweighted third-order Birch-Murnaghan EOS fit to the experimental data points.⁴³ The calculated EOS of phase B is shown as the red dashed line in (b). The insets of (b) are schematic representations of the B phase of ethane.

of the lattice parameters ($c \rightarrow a$ and $a, b \rightarrow b, c$) further justifies the argument of the close relation between the two phases. As it can be clearly seen from Fig. 4, the lattice parameters b and c become practically identical above 35–40 GPa, while the β monoclinic angle remains very close to 90° , thus making phase B effectively tetragonal under pressure. This further corroborates with the spectral discontinuities observed in the Raman spectra in the same pressure range. We conducted unweighted fits to the experimental and calculated P–V data using a third-order Birch–Murnaghan EOS⁴³ and determined the bulk modulus B and its first derivative B' at the experimental onset pressure for the A and B phases. The lattice, structural, and EOS parameters obtained in this way are given in Table I.

Figure 5 shows the proposed phase diagram of ethane, summarizing the findings of this work. Phase B representing an orientationally ordered molecular structure is stable in the whole

explored pressure range of up to 116 GPa in agreement with the theoretical predictions.²⁴

B. High-pressure study of methane

1. X-ray diffraction

The XRD data of methane of up to 117 GPa collected in this work are consistent with the I–A–B sequence of phase transformations. Concomitant Raman spectra measurements indicated that methane was in phase pre-B above 12 GPa. Our XRD data (Fig. 6) show that in the whole investigated pressure range of up to 120 GPa, the data can be indexed within a cubic structure.

These observations suggest that the simple cubic structure determined by the carbon sublattice remains stable under compression. On the other hand, previous Raman investigations show that

TABLE I. Experimental and calculated structural parameters of A and B ethane at selected pressures: space group (SG), number of formula units in the unit cell Z , lattice parameters, molecular volume, bulk modulus B , and its pressure derivative B' at the experimental onset pressure, Wyckoff site, and the corresponding coordinates as determined by *ab initio* calculations.

P (GPa)	SG	Z	a (Å)	b (Å)	c (Å)	β (deg)	V (Å ³)	B (GPa)	B'	WP	x	y	z
7 (exp)	$P4_2/mnm$	2	5.028(1)	5.028(1)	3.654(1)		46.25(5)	25.9(8)	9.2(7)				
5.9 (Ref. 19)	$P4_2/mnm$		5.092(2)	5.092(2)	3.675(18)		47.65						
30.2 (exp.)	$P2_1/n$	2	3.272(9)	4.534(5)	4.585(4)	90.44	34.11(09)	71.1(9)	3.5(17)	C(4e)	0.0586	0.3890	0.8897
30 (cal.)	$P2_1/n$	2	3.22	4.49	4.52	90.47	32.65	64	4.1	H(4e)	0.1135	0.8673	0.6282
										H(4e)	0.5630	0.6754	0.55530
										H(4e)	0.4443	0.0558	0.1745

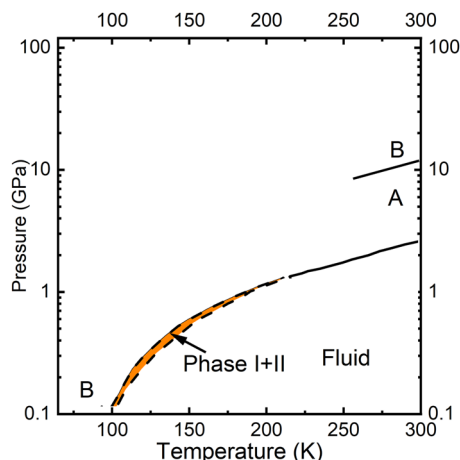


FIG. 5. Proposed P–T phase diagram of ethane according to the results of this study and Ref. 21.

there may be a variety of ordered phases, which likely occur due to different modes of orientational ordering,^{13,19,44} depending on both the sample history and pressure. For these structures, the H-positions are unknown, while C positions were determined in Ref. 9 for phase B. The investigated cubic pre-B methane, which is stable to very high pressures (see also Refs. 8 and 12), is a good proxy to determine the EOS at these conditions. We argue that pre-B, B, and HP

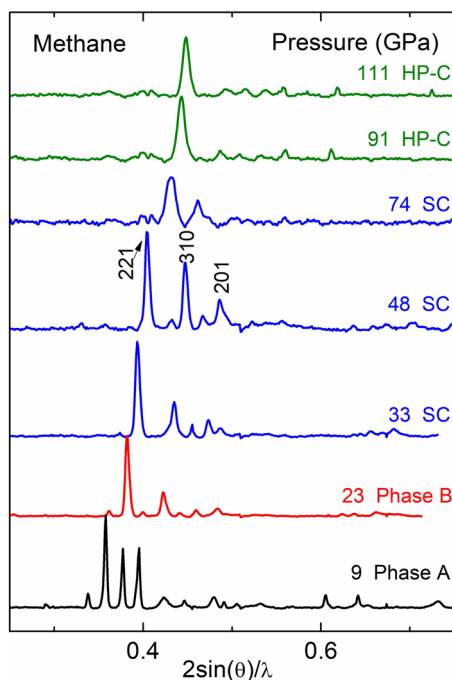


FIG. 6. Selected XRD patterns of methane at various pressures measured on the pressure increase. The corresponding Miller indices for the SC phase of methane are also noted.

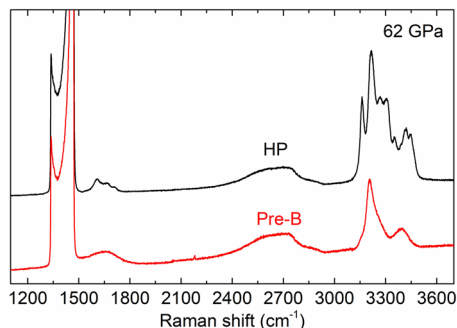


FIG. 7. Raman spectra of the pre-B and HP phases of ethane at 62 GPa, measured on two different experimental runs.

phases of methane are close in energy because from previous studies,^{13,19,44} it appears that these phases could exist (or even co-exist) at the same pressure ranges depending on the pressure–time history of the methane specimens.

2. Raman spectroscopy

Our Raman data measured concomitantly with XRD agree well with previous observations in phases I, A, B, and pre-B.^{8,15} We detected, see Fig. 7, a simple Raman spectrum of the C–H stretch modes of pre-B, which consists of two major fundamentals (ν_1 and ν_3) and a single ν_2 mode ($\approx 1600 \text{ cm}^{-1}$), in agreement with Ref. 15. On the other hand, these modes appear to be split in the HP phase, indicating a lower symmetry at the level of local order associated with the C–H bonds.

IV. DISCUSSION

Methane and ethane both are the simplest and hence the most fundamental hydrocarbons. Thus, it is vital to understand their relative thermodynamic stability at different compressions. As already mentioned in the Introduction, ethane is one of the most predictable products of chemical reactivity of methane at extreme pressures and temperatures. In order to address the issue of the relative stability of methane vs ethane and given that the PV enthalpy term plays a crucial role at high pressure, we compare the volume per molecule of methane and ethane. This is done using the simple reaction $2\text{CH}_4 \Rightarrow \text{C}_2\text{H}_6 + \text{H}_2$. Figure 8 shows the combined EOS of (a) doubled molecular volume (V_{pm}) of methane and (b) sum of the molecular volume of ethane V_{pm} plus hydrogen V_{pm} according to Loubeyre *et al.*⁴⁵ As it can be clearly seen, ethane and methane show similar compressibility, which results in similar EOSs. In details, the formation of ethane leads to increase of density at pressures below 80 GPa, but there is no discernible increase of density at higher pressures - this is equivalent to saying that the enthalpy of reaction $2\text{CH}_4 \Rightarrow \text{C}_2\text{H}_6 + \text{H}_2$ decreases with pressure up to ~ 80 GPa and remains constant at higher pressures. Therefore, ethane becomes stable already before 80 GPa.

High-temperature (HT) studies unambiguously reveal the formation of ethane, originated from methane, under high pressure–temperature conditions.^{4,6} In this case, HT commonly needed to overcome energy barriers arising from bond breaking. Moreover, previous theoretical studies strongly suggest dissociation of methane toward ethane at 95 GPa.^{5,24}

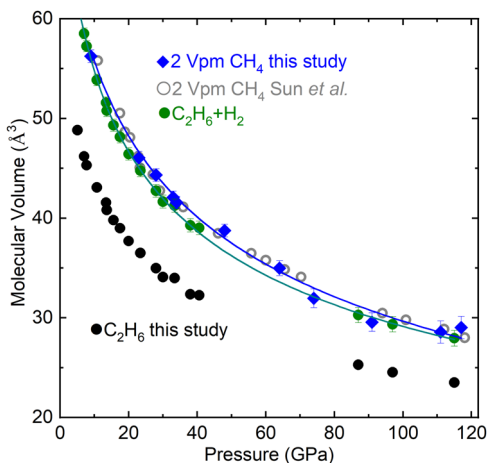


FIG. 8. Comparative equations of state of ethane (black symbols) and methane (blue symbols from our data and red symbols from Ref. 12). The EOS of methane is compared to a combined EOS of ethane (this work) and molecular hydrogen,⁴⁵ which has the same relative composition of carbon and hydrogen.

Our discussion so far did not consider the role of the entropy. Previous theoretical works (5,24) suggest that if CH_4 , C_2H_6 and H_2 are in solid phases, the entropy of the reaction $2\text{CH}_4 = \text{C}_2\text{H}_6 + \text{H}_2$ is negligible and the equilibrium pressure of this reaction is almost temperature-independent. However, when H_2 is in the fluid phase, the entropy of the right-hand side becomes much higher, and ethane formation becomes favorable at lower pressures. Indeed, experiments observe this reaction already at 2-5 GPa [4] at high temperatures.

V. SUMMARY

High-pressure phase transitions of ethane and methane have been investigated by a combined experimental (using x-ray diffraction and Raman spectroscopies) and computational (USPEX) study of up to above 100 GPa. In the case of ethane, a pressure induced phase transition was observed above 13.6 GPa, supported by both XRD and Raman measurements. The structure of this high-pressure phase, namely, phase B, was definitively determined using a combined experimental and theoretical approach; phase B appears to be isostructural to low-temperature phase III at ambient pressure known previously. This phase remains stable up to the highest pressure of this study, and a P-T phase diagram of ethane is proposed. In the case of methane, our XRD measurements revealed that in our experiments, methane followed the phase sequence $\text{I} \rightarrow \text{A} \rightarrow \text{pre-B}$, and pre-B seems to be stable to the highest pressure reached. A comparison of the ethane and methane EOSs, after adjusting the volume of ethane with hydrogen volume, revealed that there is no difference at pressures above 80 GPa, outside the experimental error, between the two volumes, i.e., $2V(\text{CH}_4)$ and $V(\text{C}_2\text{H}_6 + \text{H}_2)$ are almost the same at pressures >80 GPa. At lower pressures the formation of ethane is accompanied with density increase.

ACKNOWLEDGMENTS

A.F.G. and E.S. acknowledge support from the Army Research Office (Grant Nos. 56122-CH-H and 71650-CH) and the Deep Carbon Observatory. S.S.L. acknowledges the support from the Helmholtz Young Investigators Group CLEAR (Grant No. VH-NG-1325). Part of this work was performed at GeoSoilEnviroCARS (the University of Chicago, Sector 13), Advanced Photon Source (APS), and Argonne National Laboratory. GeoSoilEnviroCARS is supported by the National Science Foundation Earth Sciences (Grant No. EAR-1634415) and the Department of Energy GeoSciences (Grant No. DE-FG02-94ER14466). This research used resources of the Advanced Photon Source, a U.S. Department of Energy (DOE), Office of Science User Facility, operated for the DOE Office of Science by Argonne National Laboratory under Contract No. DE-AC02-06CH11357. A.R.O. and A.A.M. thank Russian Ministry of Science and Higher Education (grant H III-2711.2020.2 to leading scientific schools) for support. We acknowledge DESY (Hamburg, Germany), a member of the Helmholtz Association HGF, for the provision of experimental facilities. Part of this research was carried out at PETRA III (beamline P02.2). The research leading to these results received funding from the European Community's Seventh Framework Programme (FP7/2007-2013) under Grant Agreement No. 312284.

AUTHOR DECLARATIONS

Conflict of Interest

The authors have no conflicts to disclose.

DATA AVAILABILITY

The data that support the findings of this study are available from the corresponding author upon reasonable request.

REFERENCES

- W. B. Hubbard, *Science* **214**, 145 (1981).
- M. Podolak, A. Weizman, and M. Marley, *Planet. Space Sci.* **43**, 1517 (1995).
- F. Ancillotto, G. L. Chiarotti, S. Scandolo, and E. Tosatti, *Science* **275**, 1288 (1997).
- A. Kolesnikov, V. G. Kutcherov, and A. F. Goncharov, *Nat. Geosci.* **2**, 566 (2009).
- G. Gao, A. R. Oganov, Y. Ma, H. Wang, P. Li, Y. Li, T. Iitaka, and G. Zou, *J. Chem. Phys.* **133**, 144508 (2010).
- S. S. Lobanov, P.-N. Chen, X.-J. Chen, C.-S. Zha, K. D. Litasov, H.-K. Mao, and A. F. Goncharov, *Nat. Commun.* **4**, 2446 (2013).
- J. I. Moses, K. Rages, and J. B. Pollack, *Icarus* **113**, 232 (1995).
- H. Hirai, K. Konagai, T. Kawamura, Y. Yamamoto, and T. Yagi, *J. Phys.: Conf. Ser.* **121**, 102001 (2008).
- H. E. Maynard-Casely, C. L. Bull, M. Guthrie, I. Loa, M. I. McMahon, E. Gregoryanz, R. J. Nelmes, and J. S. Loveday, *J. Chem. Phys.* **133**, 064504 (2010).
- H. E. Maynard-Casely, L. F. Lundegaard, I. Loa, M. I. McMahon, E. Gregoryanz, R. J. Nelmes, and J. S. Loveday, *J. Chem. Phys.* **141**, 234313 (2014).
- S. Umamoto, T. Yoshii, Y. Akahama, and H. Kawamura, *J. Phys.: Condens. Matter* **14**, 10675 (2002).
- L. Sun, W. Yi, L. Wang, J. Shu, S. Sinogeikin, Y. Meng, G. Shen, L. Bai, Y. Li, J. Liu, H.-k. Mao, and W. L. Mao, *Chem. Phys. Lett.* **473**, 72 (2009).
- P.-N. Chen, C.-S. Zha, X.-J. Chen, J. Shu, R. J. Hemley, and H.-k. Mao, *Phys. Rev. B* **84**, 104110 (2011).
- Q. Zhu, A. R. Oganov, C. W. Glass, and H. T. Stokes, *Acta Crystallogr., Sect. B: Struct. Sci.* **68**, 215 (2012).

- ¹⁵J. E. Proctor, H. E. Maynard-Casely, M. A. Hakeem, and D. Cantiah, *J. Raman Spectrosc.* **48**, 1777 (2017).
- ¹⁶H. Kadobayashi, H. Hirai, H. Ohfuji, M. Ohtake, M. Muraoka, S. Yoshida, and Y. Yamamoto, *J. Chem. Phys.* **152**, 194308 (2020).
- ¹⁷S. B. Hansen, R. W. Berg, and E. H. Stenby, *Appl. Spectrosc.* **55**, 745 (2001).
- ¹⁸R. M. Hazen, H. K. Mao, L. W. Finger, and P. M. Bell, *Appl. Phys. Lett.* **37**, 288 (1980).
- ¹⁹R. Bini and G. Pratesi, *Phys. Rev. B* **55**, 14800 (1997).
- ²⁰A. V. Kurnosov, A. G. Ogienko, S. V. Goryainov, E. G. Larionov, A. Y. Manakov, A. Y. Lihacheva, E. Y. Aladko, F. V. Zhurko, V. I. Voronin, I. F. Berger, and A. I. Ancharov, *J. Phys. Chem. B* **110**, 21788 (2006).
- ²¹M. Podsiadło, A. Olejniczak, and A. Katrusiak, *Cryst. Growth Des.* **17**, 228 (2017).
- ²²L. Q. Read, J. E. Spender, and J. E. Proctor, *J. Raman Spectrosc.* **51**, 2311 (2020).
- ²³M. S. Somayazulu, L. W. Finger, R. J. Hemley, and H. K. Mao, *Science* **271**, 1400 (1996).
- ²⁴A. S. Naumova, S. V. Lepeshkin, and A. R. Oganov, *J. Phys. Chem. C* **123**, 20497 (2019).
- ²⁵L. Spanu, D. Donadio, D. Hohl, E. Schwegler, and G. Galli, *Proc. Natl. Acad. Sci. U. S. A.* **108**, 6843 (2011).
- ²⁶N. A. Klimenko, N. N. Gal'tsov, and A. I. Prokhvatilov, *Low Temp. Phys.* **34**, 1038 (2008).
- ²⁷G. J. H. Van Nes and A. Vos, *Acta Crystallogr., Sect. B: Struct. Crystallogr. Cryst. Chem.* **34**, 1947 (1978).
- ²⁸K. Syassen, *High Pressure Res.* **28**, 75 (2008).
- ²⁹M. Matsui, *J. Phys.: Conf. Ser.* **215**, 012197 (2010).
- ³⁰C. Prescher and V. B. Prakapenka, *High Pressure Res.* **35**, 223 (2015).
- ³¹W. Kraus and G. Nolze, *J. Appl. Crystallogr.* **29**, 301 (1996).
- ³²A. C. Larson and R. B. V. Dreele, GSAS: General structure analysis system, Technical Report No. LAUR 86-748, Los Alamos National Laboratory, 2000.
- ³³A. Boultif and D. Louër, *J. Appl. Crystallogr.* **37**, 724 (2004).
- ³⁴A. R. Oganov and C. W. Glass, *J. Chem. Phys.* **124**, 244704 (2006).
- ³⁵A. K. Rappe, C. J. Casewit, K. S. Colwell, W. A. Goddard, and W. M. Skiff, *J. Am. Chem. Soc.* **114**, 10024 (1992).
- ³⁶G. Kresse and J. Hafner, *Phys. Rev. B* **47**, 558 (1993).
- ³⁷G. Kresse and J. Furthmüller, *Comput. Mater. Sci.* **6**, 15 (1996).
- ³⁸G. Kresse and J. Furthmüller, *Phys. Rev. B* **54**, 11169 (1996).
- ³⁹J. P. Perdew, K. Burke, and M. Ernzerhof, *Phys. Rev. Lett.* **77**, 3865 (1996).
- ⁴⁰S. Grimme, J. Antony, S. Ehrlich, and H. Krieg, *J. Chem. Phys.* **132**, 154104 (2010).
- ⁴¹G. Kresse and D. Joubert, *Phys. Rev. B* **59**, 1758 (1999).
- ⁴²K. Van Helvoort, W. Knippers, R. Fantoni, and S. Stolte, *Chem. Phys.* **111**, 445 (1987).
- ⁴³F. Birch, *J. Geophys. Res.* **83**, 1257, <https://doi.org/10.1029/jb083ib03p01257> (1978).
- ⁴⁴R. Bini, L. Ulivi, H. J. Jodl, and P. R. Salvi, *J. Chem. Phys.* **103**, 1353 (1995).
- ⁴⁵P. Loubeyre, R. LeToullec, D. Hausermann, M. Hanfland, R. J. Hemley, H. K. Mao, and L. W. Finger, *Nature* **383**, 702 (1996).